Comparative analysis of mechanical strength of diamond-sawn silicon wafers depending on saw mark orientation, crystalline nature and thickness

Louise Carton, Roland Riva, Fabrice Coustier, Amal Chabli, Daniel Nelias, Marion Fourmeau

Comparative analysis of mechanical strength of diamond-sawn silicon wafers depending on saw mark orientation, crystalline nature and thickness

Louise Carton [a,b,*], Roland Riva [a], Daniel Nelias [c], Marion Fourmeau [c], Fabrice Coustier [a], Amal Chabli [a]

[a] *Univ Grenoble Alpes, CEA-LITEN, INES, 50 avenue du Lac Léman, F-73375 Le Bourget-du-Lac, France*

[b] *Agence de l'environnement et de la Maîtrise de l'Energie 20 avenue du Grésillé - BP 90406 49004 Angers Cedex 01 France*

[c] *Univ Lyon, INSA-Lyon, CNRS UMR5259, LaMCoS, F-69621, France*

* Corresponding author.

Email addresses: louise.carton@cea.fr (L. Carton), roland.riva@cea.fr (R. Riva), daniel.nelias@insa-lyon.fr (D. Nelias), marion.fourmeau@insa-lyon.fr (M. Fourmeau), fabrice.coustier@cea.fr (F. Coustier), amal.chabli@cea.fr (A. Chabli)

Declarations of interest: none.

ABSTRACT

Reducing the as-cut thickness of silicon wafers is one of the key issues to significantly lower the manufacturing costs of the photovoltaic industry. The pursuit of this objective is encouraged by the outstanding development of diamond wire sawing technology, which in addition to being twice more productive, also has great potential for further kerf reduction. However, in order to avoid higher breakage rates, it is crucial to understand how the sawing process affects the mechanical resistance of wafers as their thickness decreases. In this study, wafers of 180, 160 and 140 µm thickness were cut out of monocrystalline and multicrystalline silicon bricks. Their mechanical strength was evaluated by performing 4-line bending tests coupled with finite element simulations. The specimens were loaded in the parallel and perpendicular direction with respect to the saw marks. Because of the particular shape and orientation of the sawing-induced defects, all tested wafers are significantly weaker in parallel loading. While monocrystalline and multicrystalline wafers exhibit similar mechanical strength when bent perpendicular to the sawing marks, multicrystalline wafers are 30% less resistant in parallel loading. Finally, it is shown that the fracture stress of a wafer of a given silicon quality is independent of its thickness.

KEYWORDS

- Silicon wafers
- Diamond wire sawing
- 4-line bending test
- Finite element simulation
- Fracture strength

1. Introduction

For several years now, the photovoltaic (PV) industry and research has been under considerable pressure to reduce the production costs at every stage of the manufacturing chain. Although there has been some effort to introduce new materials [1,2], silicon-wafer-based cells continue to largely dominate the solar market. With approximately 50% of today's solar cell price assigned to the wafer itself [3], reducing the as-cut thickness of silicon wafers is becoming a critical objective. Wafers are obtained by slicing silicon bricks with a multi-wire saw, with standard thickness around 180 µm. Lowering this value down to 140 µm would yield in 17% more wafers obtained from the same brick.

In this context, diamond wire sawing (DWS) technology has made outstanding progress in the PV industry over the last few years, gradually replacing the historical loose abrasive slurry (LAS) sawing technique. LAS involves cutting silicon with abrasive silicon carbide particles suspended in a fluid and driven by a steel wire. Although LAS technology has proved its worth, its potential improvements are too limited to meet the objectives of wafering cost reduction. In contrast, DWS technique, which uses a wire coated with diamond grits, provides many advantages, such as the ability to cut at least twice faster [4]. Moreover, the wire core, which is already much thinner than for LAS, still has great potential for further diameter decrease and hence material loss reduction. DWS also facilitates the recycling of the silicon wasted during cutting (kerf) [5]. As of today, DWS has already become the predominant technology for cutting monocrystalline silicon (mono-Si). The technology still faces some challenges when it comes to multicrystalline silicon (mc-Si), mainly because the presence of crystallographic defects (dislocations, grain/twin boundaries) makes it more difficult to cut than mono-Si [6], and because the surface structure of diamond-sawn mc-Si wafers requires a modification of the texturization process [7]. This is why LAS still accounts for a substantial proportion of the industrial sawing of mc-Si wafers, especially with the recent introduction of structured wire, which enables to double the process efficiency while maintaining a very good wafer quality [8,9]. However, many studies focus on overcoming the hurdles encountered by DWS of mc-Si [10–12], as it presents a strong cost-effective advantage compared to mono-Si. Therefore, current trends indicate that DWS should very quickly gain market share for mc-Si wafers as well [13].

There is no question that DWS is a compelling solution to achieve significant wafer thickness reduction. However, the abrasion mechanism involved in this process is fundamentally different from LAS technology and therefore generates very specific surface and subsurface damage [14,15], which directly influence the mechanical integrity of the wafers. Slicing action in DWS occurs via the combined scratching and indenting actions of the fixed diamond abrasives on the silicon surface. The surfaces thus generated exhibit long parallel grooves oriented in the direction of the wire as well as randomly distributed indentation pits [16], which are characteristic of a mixture of ductile material removal and brittle fracture [17,18]. Recent studies focus on studying the influence of various sawing parameters that favor ductile mode cutting over brittle chipping [19], as it is known to play an important role in the quality of as-cut surfaces [20]. The material removal mode is mainly investigated through scribing experiments using single diamond indenters [21], or even a small section of actual diamond wire [22]. The most recent works have shown that the shape and the wear of the abrasive [12,23,24], the wire speed [25,26], as well as the cutting fluid used in the process [27], are some of the important parameters that influence the quality of silicon wafer surfaces.

Many studies also aim at directly linking the surface and subsurface damage of the diamond-sawn wafers with their mechanical properties. In particular, several works highlighted that the saw marks left at the wafer surface by the back-and-forth movement of the wire cause an anisotropy of fracture strength depending on the loading direction [16,28]. Some interesting studies showed that this anisotropy could be significantly reduced, or even suppressed, by

removing the surface damage layer by chemical etching [29,30]. Beyond the sawing-induced defects, which can be considered as extrinsic factors, prior work has shown that fracture strength of silicon wafers is also dependent on intrinsic factors, such as non-uniform residual stress caused by solidification [31,32], grain or twin boundaries [33], and bulk defects such as dislocations [34] or inclusions [35].

While the study of the mechanical integrity in the PV field has recently extended to solar cells [36] and modules [37], there is almost no existing work focusing on the mechanical properties of diamond-sawn as-cut thin wafers. Knowing that the time when a wafer is most likely to break is in the as-cut state, it is essential to understand if the sawing induced damage for thinner wafers could become critical and lead to greater breakage rates during the following handling steps.

In this study, we therefore propose a rigorous analysis to evaluate the mechanical strength of diamond-sawn wafers of different thicknesses and silicon qualities.

2. Materials consideration

The wafers used in this investigation were obtained from a Czochralski grown mono-Si ingot and a directionally solidified high-performance mc-Si ingot. Two bricks extracted from each ingot were cut with a diamond wire saw using a special wire guiding system with a variable pitch, which enables the slicing of wafers of three different thicknesses (180, 160 and 140 µm) along the entire brick length, as shown in Fig. 1. The mono-Si and mc-Si brick were cut in the exact same operating conditions and with the same wire (80 µm core diameter and 8-16 µm diamonds), with the exception of the wire consumption (1 m/wafer and 2 m/wafer for the mono-Si and mc-Si brick, respectively). Introducing more new wire when sawing mc-Si is indeed necessary ensure the cutting effectiveness, because the diamond wire wears more quickly than with mono-Si. Kumar et al. [12] recently demonstrated with scribing experiments that the localized defects in mc-Si such as grains and twin boundaries were responsible for higher scribing forces and therefore greater wear of the diamond particles.

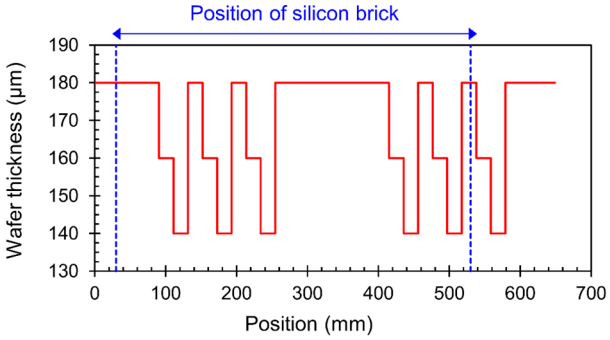

Fig. 1. Nominal wafer thickness along a brick cut with the special wire guiding system

The 156 x 156 mm wafers used for this study were taken from the fresh wire side of the bricks, i.e. where the new wire first enters the brick and is therefore the least worn. Approximately 80 neighboring wafers per brick and thickness were collected directly after the slicing process, with no chemical or texturing treatment applied to the samples. The as-cut thickness and total thickness variation (TTV) of each wafer were measured using E+H Metrology's model "MX-204-8-49-q". This technology uses capacitive sensors to measure the local thickness at 45 or 49 points (for pseudo-square mono-Si wafers or square mc-Si wafers respectively) evenly distributed on the wafer surface. The as-cut thickness of the entire wafer is then calculated as the average of the 45 (or 49) values, and the TTV as the difference between the largest and smallest value. The mean values and standard deviations of each set are listed in Table 1.

Table 1
Mean thickness and TTV of each set of wafers (80 wafers per series)

Silicon brick	Nominal thickness (µm)	Mean thickness ± standard deviation (µm)	Mean TTV ± standard deviation (µm)	Number of measuring points per wafer
mono-Si	140	138.9 ± 0.7	4.7 ± 1.2	45
mono-Si	160	158.6 ± 0.5	4.9 ± 1.1	45
mono-Si	180	178.3 ± 0.5	4.5 ± 1.2	45
mc-Si	140	139.0 ± 1.5	12.5 ± 3.7	49
mc-Si	160	159.0 ± 1.1	11.1 ± 3.3	49
mc-Si	180	178.4 ± 0.8	8.6 ± 1.5	49

On both mono-Si and mc-Si wafers, the characteristic parallel saw marks caused by the back-and-forth movement of the diamond wire are well observable with the naked eye (Fig. 2).

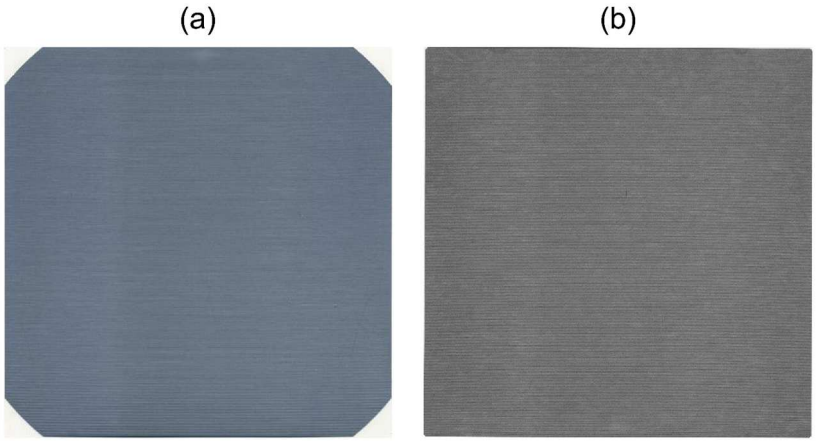

Fig. 2. Scanning images of a diamond wire sawn mono-Si (a) and mc-Si (b) wafer

In order to perform an accurate comparison of the different sets of wafers, it is necessary to consider the different material stiffnesses of mono-Si and mc-Si. On the one hand, due to the cubic symmetry of the crystal lattice, mono-Si exhibits indeed an anisotropic behavior, which can be described by the fourth-order stiffness tensor $\mathbf{C}$ owning three independent parameters C_{11}, C_{12} and C_{44} in the crystallographic coordinate system of principal axes [100], [010] and [001]. At room temperature and ambient pressure, the measurements considered as the most accurate in the literature were reported by Hall [38] with sound-velocity measurements and are recalled below:

$$\mathbf{C} = \begin{pmatrix} 165.7 & 63.9 & 63.9 & & & \\ 63.9 & 165.7 & 63.9 & & & \\ 63.9 & 63.9 & 165.7 & & & \\ & & & 79.6 & & \\ & & & & 79.6 & \\ & & & & & 79.6 \end{pmatrix} \textit{(GPa)}$$

Based on the orthotropic nature of this tensor, it can be deduced that the smallest value of Young's modulus is 130 GPa (along the [100] directions) and the greatest is 188 GPa (along the [111] directions).

On the other hand, as an aggregate of multiple single crystals separated by grain boundaries, mc-Si theoretically owns an intermediate value of Young's modulus between 130 GPa and 188 GPa. If the average grain size is negligible compared to the dimensions of the sample, the multi-crystal can be homogenized into an isotropic material with only two

parameters, the Young's modulus and the Poisson's ratio. Funke et al. [39] performed an analytical calculation considering a uniform orientation distribution of the grains in a representative volume element and obtained E = 162.5 GPa and ν = 0.223. A different approach, based on a numerical model in which the grain structure of the wafer is generated by a Voronoi tessellation, was proposed by Zhao et al. [40]. The resulting wafer is thereafter introduced in a finite element model reproducing a 4-line bending test, and the equivalent Young's modulus, calculated from the slope of the load-deflection curve, is assessed as 163 ± 2 GPa. Given the negligible difference in value between the two methods, it can be concluded that the homogenization hypothesis made by Funke et al. is correct, and in the following study the elastic behavior of mc-Si wafers is characterized by the values E = 162.5 GPa and ν = 0.223. The experimental and finite element simulation results presented in this study show that these values are accurate.

3. Experimental procedure

3.1. Surface characterization

A 3D laser confocal microscope (Plu Neox - 3D Optical Profiler from Sensorfar) was used to analyze the surface topography and measure the areal surface roughness Sa and the maximum peak-to-valley roughness height Sz of the wafer samples. In order to obtain results as representative as possible, five wafers of 180 µm and five wafers of 140 µm from each silicon type were observed. For each single wafer, images were taken at five different areas of the plate (center, top left, top right, bottom right and bottom left). Each image was moreover taken with the lowest magnification (x20, corresponding to a spot size of 636 x 477 µm) as well as with the highest magnification (x100, corresponding to a spot size of 127 x 95 µm). Thus, for a given thickness, silicon type and magnification level, 25 images were obtained (5 wafers x 5 measuring areas), allowing a statistical treatment of the roughness measurement data.

3.2. Test method

Various test methods are available to characterize the strength of brittle materials such as silicon, including twist tests [41,42] or biaxial bending tests like the Ring-on-Ring [43] or Ball-on-Ring method [44]. However, for testing photovoltaic silicon wafer strength, the uniaxial 4-line bending setup is the most commonly used in literature, as it enables to have a large area of the wafer submitted to a uniform mechanical state [10]. Indeed, between the two central contact lines, the load occurs as a homogeneous tensile stress on the bottom surface of the wafer and a compression stress on the top surface. This method was therefore chosen to evaluate the mechanical strength of the as-cut wafers in this work.

While a few studies choose to rely on the standard test method for advanced ceramics [45] to design their 4-line bending setup [40,46], their recommendations are often not suited to the geometry of photovoltaic silicon wafers, which have an extremely high length-to-thickness ratio (> 10^3 in the case of 140 µm wafers). In order to overcome this issue, a standard test method for strength testing of photovoltaic wafers was recently developed, which provides appropriate requirements for the dimensions and testing conditions of the 4-line bending setup [47]. However, the distance between support and loading rollers recommended in the standard for thin wafers (80 - 40 mm) was unsuitable for this work, as it did not enable to reach the breaking point of some of the 140 µm wafers. An optimal distance between the support and loading rollers was therefore determined experimentally, with the aim of reaching failure for all wafers (from 180 to 140 µm) while still maintaining an inner span as large as possible in order to evaluate a greater area.

The inner and outer spans were thus chosen to be 48 and 80 mm, respectively (Fig. 3). The support and loading devices of the setup are cylindrical rollers with a diameter of 8 mm. The displacement of the loading rollers is imposed, and both the force and displacement are recorded during the test. The measuring range of the load cell reaches 50 N. A crosshead

speed rate of 10 mm/min is used (in agreement with [47]), which implies a strain rate in the order of 10^{-5} s^{-1} and thus a quasi-static loading condition.

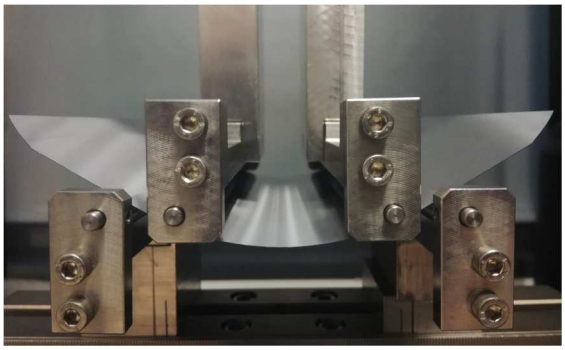

Fig. 3. Picture of the 4-line bending setup used to test the silicon wafers

In order to account for the surface anisotropy of the wafers, each set was further divided into two subsets to be tested in two different configurations: with the saw marks parallel and perpendicular to the loading rollers (thereafter referred to as *wire direction* and *cut direction*, respectively). In order to avoid the risk of having one series with a different crystallographic structure and therefore different mechanical properties, the two subsets were alternately sampled, as illustrated in Fig. 4.

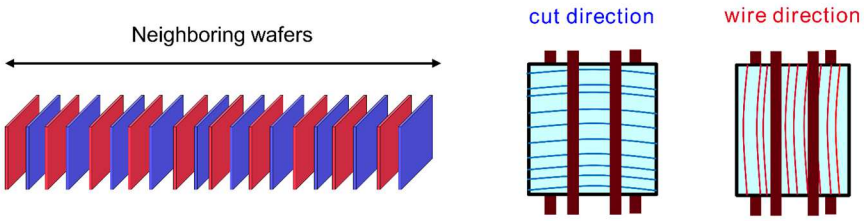

Fig. 4. Sampling methodology applied to each set of wafers to be tested with the 4-line bending setup

For each set of wafers of a given thickness and silicon type, 40 samples per direction were tested until fracture. The raw results are obtained as load-deflection curves, and the values of fracture displacement (δ_{break}) and fracture force (F_{break}) are stored as output data for each wafer. The curves registered for the mono-Si and mc-Si wafers of the three different thicknesses are depicted in Fig. 5 for the *cut direction*.

The mc-Si samples exhibit a stiffer behavior than the mono-Si ones. This can be explained by the above-mentioned differences in material elasticity. Indeed, in the 4-line bending setup, the mono-Si wafers are loaded in the [100] directions (regardless of the saw marks orientation) and thus exhibit a Young's modulus of 130 GPa, whereas the mc-Si wafers are characterized by an equivalent Young's modulus of approximately 163 GPa. This ratio of 1.25 can be found back when comparing the slopes of the curves, thereby corroborating the accuracy of the Young's modulus value chosen to characterize the mc-Si wafers.

As could be expected, the maximum deflections of the wafers before fracture increase with decreasing thicknesses, reaching 20 mm for 140 µm mono-Si wafers. The higher stiffness of mc-Si wafers justifies the lower deflection values. It can also be observed that the mc-Si curves show a greater scattering, especially for thinner wafers. This can be explained by the stronger variation in thickness of the mc-Si wafers (Table 1).

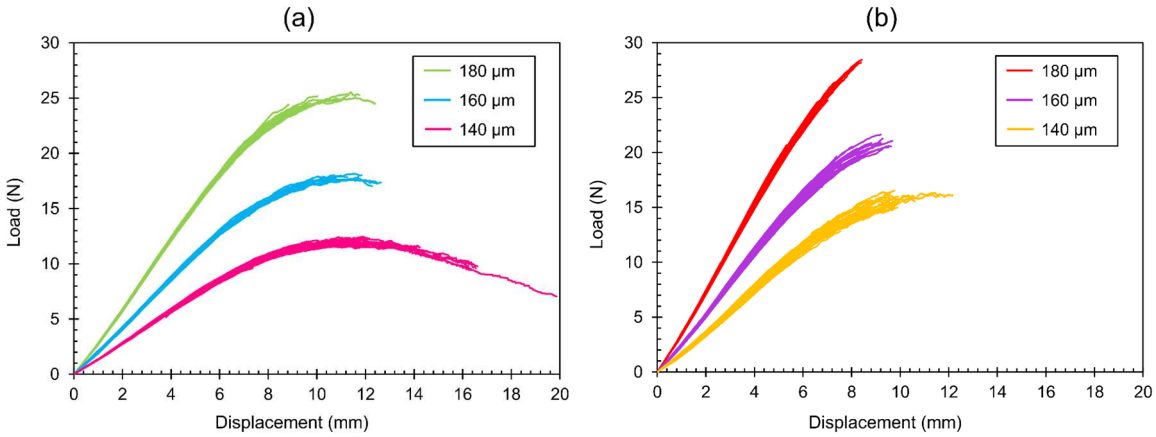

Fig. 5. Measured load-deflection curves obtained for (a) mono-Si and (b) mc-Si wafers of the three thicknesses tested in 4-line bending in the *cut direction* (40 samples each)

3.3. Numerical simulation

In order to assess the mechanical strength of wafers of different materials and thicknesses, the knowledge of the stress distribution in the sample at the time of fracture is required. Because of the non-linearity of the load-deflection curves, the analytical formulas expressing stress as a function of load are not valid in this study. The reasons for this non-linearity are mainly the large displacements reached by the samples before failure, as well as the frictional contact between the wafer and the rollers. A finite element (FE) model of the experimental setup was therefore developed on ANSYS software. The FE analysis is purely elastic and does not include fracture mechanics simulation.

In order to optimize the calculation time, the double symmetry of the 4-line bending setup was considered and only a quarter of the geometry was modeled in 3D. The silicon wafer is meshed with quadratic cubic elements, with 6300 elements on the surface and 4 along the thickness, having an aspect ratio ranging from 70:1 in the areas where the mesh is the least refined to 10:1 where the mesh is the most refined, at the contact regions (Fig. 6.a.). The rollers are modeled as semi-cylindrical rigid surfaces. The supporting rollers are fixed in all degrees of freedom, and a displacement is imposed on the loading rollers. The analysis performed is static, i.e. inertia and damping effects are not considered. In order to account for the changes in stiffness during the deformation process of the wafer, the large deflection formulation is implemented. The frictional contact between the rollers and the wafer surface is computed using the Augmented Lagrange algorithm. Depending on the crystallinity of the tested silicon samples, two behaviors are considered for the wafer material in the simulation. For the mono-Si wafers, the anisotropic elasticity is defined by the above-mentioned stiffness tensor. For the mc-Si wafers, the material is considered as isotropic with a Young's modulus of 162.5 GPa and a Poisson's ratio of ν = 0.223. A total displacement of 20 mm of the loading rollers is imposed for all simulations, which corresponds to the maximal value reached in the experimental setup. The calculated wafer deflection corresponding to this value is shown in Fig. 6.b. The symmetry expansion has been applied on the model for a better representation of the whole wafer deflection.

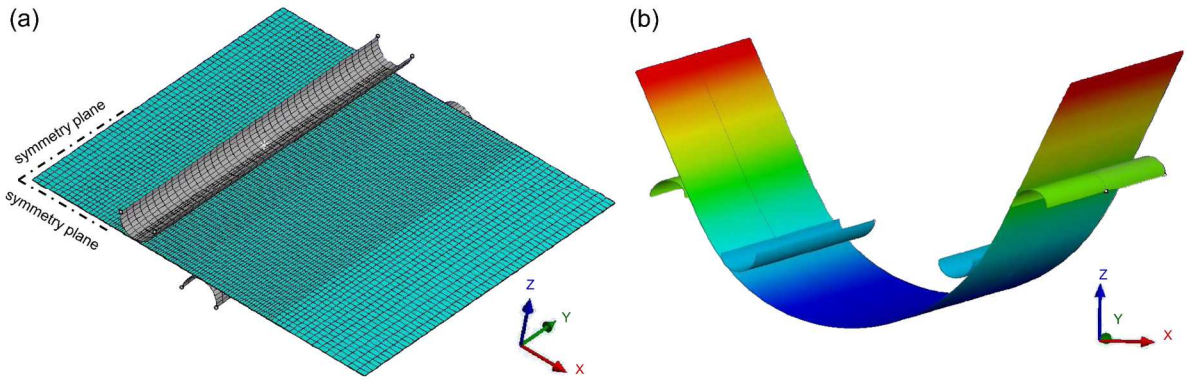

Fig. 6. (a) Mesh used for the FE model of the 4-line bending test and (b) Calculated deflection of a monocrystalline wafer for a displacement of the loading rollers of 20 mm

Given that the only unknown parameter in the experimental setup is the coefficient of friction of the contact between rollers and wafer, its value was varied empirically until the numerical and experimental load-deflection curves showed good agreement. In order to validate the accuracy of the model, we simulated the minimal and maximal thickness of each set of wafers of a given nominal thickness and silicon material, as illustrated in Fig. 7.

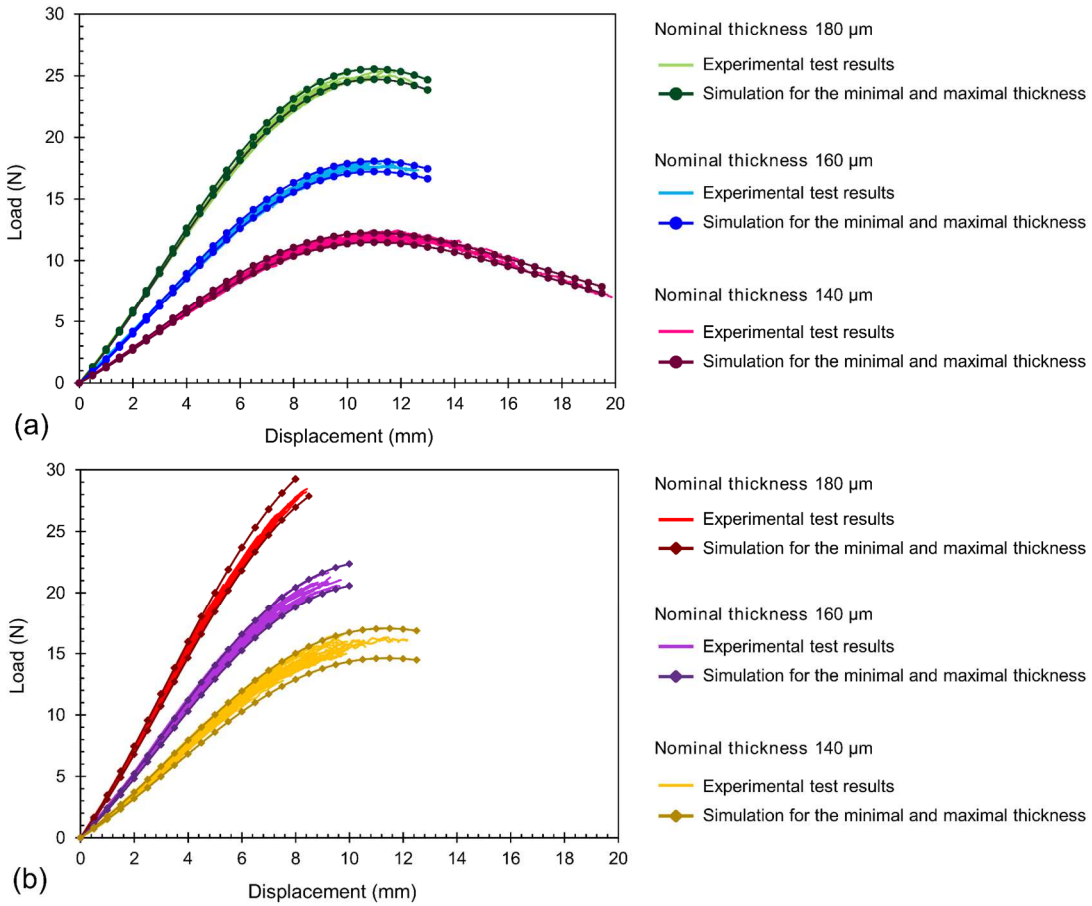

Fig. 7. Comparison of experimental load-displacement curves with the results of the simulation for (a) mono-Si and (b) mc-Si wafers of three different nominal thicknesses

For the set of mono-Si wafers, a friction coefficient of f = 0.1 in the simulations showed the best agreement with the experimental curves for all thicknesses. For the set of mc-Si wafers, a reasonably good match was obtained with the same coefficient value for the 180 and 160 µm wafers, but the simulations of the 140 µm wafers showed better agreement with the experimental curves when a coefficient of friction of f = 0.15 was employed. It is assumed

that this difference in behavior came from a minor blocking defect in the experimental setup when testing these particular series, which was detected afterwards. This variation in friction coefficient value has however very little influence on the calculation of the stresses in the wafer. It was indeed shown that the maximum difference between the calculated stress value for a friction coefficient 0.1 and 0.15 is less than 4%. The FE model was therefore validated as an accurate interpretation tool to compute the stresses in the mono-Si and mc-Si wafers from the experimental results obtained.

The analysis of the calculated stress field confirms that the wafer is subjected to a uniaxial uniform stress between the loading rollers, and that the stress outside the supporting rollers is zero. Because silicon is a brittle material, the failure criterion used to determine the stress at the time of breakage is the maximum principal stress. The calculation of the breakage stresses from the experimental results is then done as follows: for each set of wafers of a given nominal thickness and material, five thicknesses within the measured range of the series are simulated to obtain the corresponding stress-displacement curves $\sigma = f(\delta)$. The charts of the other thicknesses are then interpolated based upon the calculated results. These curves are then used to compute the maximal breakage stress of each sample, knowing its thickness and the value of the fracture displacement: $\sigma_{max} = f(\delta_{break})$.

3.4. Statistical evaluation

The breakage stress values obtained for a series of identical wafers show a large scattering. This dispersion results from the brittle nature of silicon, which is composed of multiple defects acting as stress concentrators. The fracture strength of a silicon wafer is thus ultimately controlled by the density, size and geometry of its defects, which can vary strongly even within a single series. The mean stress value is therefore not sufficient to represent the strength of a set of wafers and the values require statistical treatment. Weibull theory for brittle fracture [48] is based on the weakest link hypothesis, according to which the survival probability of a body is the product of survival probabilities of each volume element within the body, so that failure of the whole solid occurs as soon as the material strength is surpassed at one element containing the critical defect. In this study, we fitted the results to a two-parameter Weibull distribution, in which the probability of failure P_f at an applied stress σ is defined as:

$$P_f(\sigma) = 1 - \exp\left[-\left(\frac{\sigma}{\sigma_\theta}\right)^m\right] \quad (1)$$

where σ_θ represents the characteristic fracture strength at which 63.2% of the samples will fail, and *m* is the Weibull modulus, which describes the scattering of the results (a higher value of *m* means a small variation in strength and vice versa). The Weibull parameters were estimated with the maximum likelihood method and the confidence bounds were calculated with the Fisher matrix method for a confidence level of 90%.

3.5. Fracture pattern investigation

Destructive mechanical testing such as the 4-line bending setup used in this study enables to assess the mechanical strength, maximal deflection and load applicable to a wafer. However, it does not provide information regarding the way wafers are cracking, nor the origin of the crack that led to the failure of the sample. Indeed, the wafers usually break abruptly and shatter into many small fragments, thus making a visual analysis impossible.

An experimental technique allowing to maintain the silicon fragments after failure was therefore implemented. Prior to testing, some wafers are prepared as illustrated in Fig. 8: a plastic film is positioned on one side of the sample and held to the surface by capillarity with a few drops of water (1). The wafer is then turned upside down and another plastic film is placed similarly on the opposite side (2). When the wafer thus prepared (3) is tested until failure, the fragments remain between the plastic films. The samples can then be observed

with integrated photoluminescence imaging in order to visualize the fracture pattern. As this preparation step is time-consuming, it was only applied on a few chosen samples. A preliminary study on 10 adjacent 140 µm mono-Si wafers was carried out, where half of the samples were prepared with plastic films and the other was left unchanged. The comparison of the experimental curves showed that the presence of the plastic films on the wafers has no significant influence either on their elasticity, or on the fracture displacement values (Fig. 9).

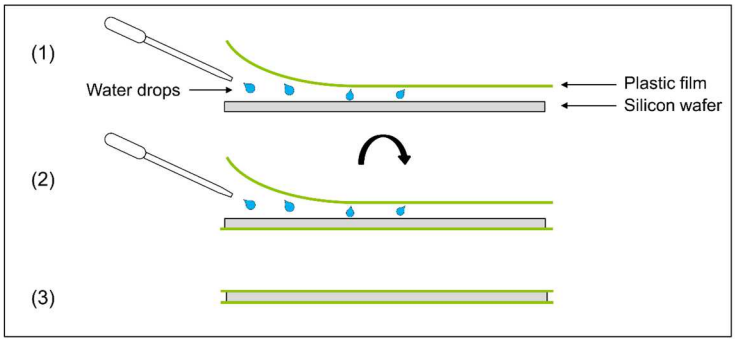

Fig. 8. Schematic of the sample preparation procedure implemented to maintain fragments after failure of the wafer

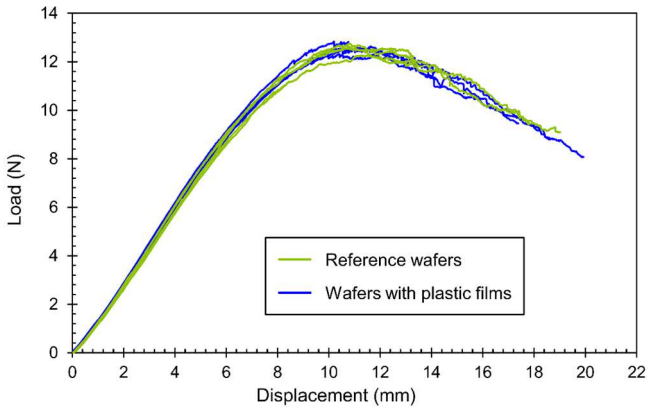

Fig. 9. Measured load-displacement curves obtained for 140 µm mono-Si wafers with and without the plastic films preparation

4. Results and discussion

4.1. Surface morphology

Examples of 3D surface profiles obtained with the confocal microscope are shown in Fig. 10 for a mono-Si and mc-Si wafer of thickness 140 µm, at magnification x20 and x100. The surfaces exhibit the characteristic parallel long grooves resulting from the scratching of the diamond particles and the ductile mode deformation of silicon [29]. These grooves are sometimes interrupted by unevenly scattered indentation pits, which were created when small silicon chips were broken off from the surface [14]. As can be seen on Fig. 10, mono-Si and mc-Si wafers show very similar surface characteristics. The same observation can be done on all images obtained and is confirmed by the roughness parameters extracted from the surface profiles, which are summarized for all wafers observed in Table 2. In comparison with the scattering of the parameter values, it can be observed that there is no statistically significant difference in roughness between mono-Si and mc-Si wafers. This is true regardless of the thickness (140 or 180 µm) and the magnification used (x20 or x100).

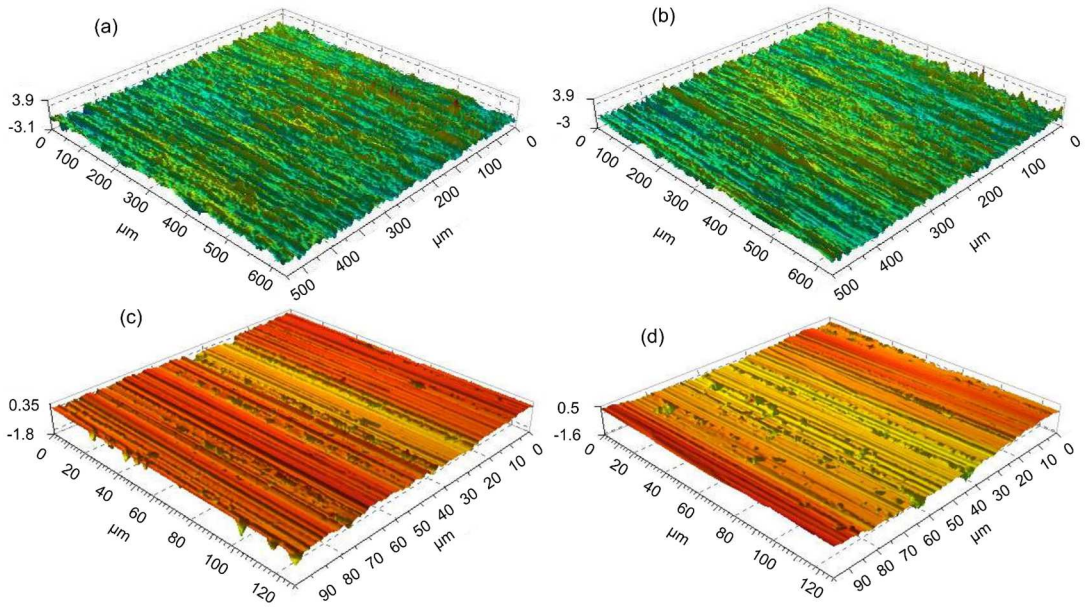

Fig. 10. Topographical maps of 140 µm wafers at magnification x20 (top row) and x100 (bottom row) for mono-Si (a and c) and mc-Si (b and d)

Table 2
Areal surface roughness Sa and maximum peak-to-valley Sz measured with confocal microscopy at magnification x20 and x100 on mono-Si and mc-Si wafers of thicknesses 140 and 180 µm (mean values and standard deviation based on 25 measurements)

Magnification	Nominal thickness	Silicon-type	Mean Sa ± standard deviation (µm)	Mean Sz ± standard deviation (µm)
x 20	140 µm	mono-Si	0.44 ± 0.10	6.38 ± 2.01
		mc-Si	0.43 ± 0.06	5.60 ± 1.07
	180 µm	mono-Si	0.47 ± 0.05	6.31 ± 1.64
		mc-Si	0.45 ± 0.05	6.56 ± 1.76
x 100	140 µm	mono-Si	0.11 ± 0.02	2.17 ± 0.68
		mc-Si	0.12 ± 0.03	2.02 ± 0.50
	180 µm	mono-Si	0.12 ± 0.03	2.30 ± 0.48
		mc-Si	0.12 ± 0.03	2.19 ± 0.73

The roughness parameters and surface profiles are thus comparable for all wafers analyzed, regardless of their thickness and silicon type. Therefore, in spite of their differences in crystallinity, mono-Si and mc-Si wafers exhibit similar surface morphologies after sawing. This observation agrees with the findings of Kumar et al., who showed that for a given abrasive shape, the scribed surface morphologies of mono-Si and mc-Si were very similar [22]. More precisely, they found that the morphology was more dependent on the grit shape than on crystallographic orientation. Both our results seems to indicate that the as-cut surface morphology of a wafer is mainly defined by the characteristics of the cutting wire, particularly the shape and size of the abrasives used, and not really by the crystallinity of the silicon brick.

4.2. Mechanical strength

By means of the FE models presented in Section 3.3, the fracture stresses were calculated from the experimental results. These stresses were then used to estimate the Weibull parameters for all tested series, which are presented in Table 3 and depicted as Weibull probability plots in Fig. 11. It is worth noting that the experimental and sampling methods employed in this study allow studying the influence of various parameters on the mechanical

properties. First, we consider the influence of the bending orientation with respect to the sawing marks. Then, since the wafers of different thicknesses were cut out of the same silicon brick and possess therefore the same material properties, we are able to study the influence of the thickness alone. Finally, because the mono-Si and mc-Si bricks were cut using the same processing parameters, we are in a position to evaluate the influence of the silicon crystallinity on the mechanical properties of the wafers.

4.2.1. Influence of the saw marks orientation

The results firstly confirm the well-known dependency of the mechanical strength on the orientation of the marks: wafers are much stronger in the *cut direction*. This difference is even more critical for mc-Si wafers: they are three times weaker when loaded in the *wire direction*, while mono-Si wafers are only twice weaker. The loading direction also has an influence on the scattering of the results: the calculated Weibull modulus of wafers loaded in the *wire direction* is on average twice the one from wafers tested in *cut direction*, for both mono-Si and mc-Si wafers.

Table 3
Weibull parameters of strength with 90% confidence bounds of mono-Si and mc-Si wafers of different thicknesses tested in 4-line bending in *wire* and *cut direction*

Silicon type	Nominal thickness	Testing direction	σ_θ (MPa)	m (-)
mono-Si	180 µm	*Wire*	113 (111…115)	14.4 (11.5 … 18.1)
		Cut	251 (238 … 265)	5.3 (4.2 … 6.7)
	160 µm	*Wire*	119 (117 … 121)	15.8 (12.7 … 19.8)
		Cut	246 (236 … 256)	7.2 (6.7 … 9.1)
	140 µm	*Wire*	119 (117 … 121)	18 (14.3 …22.7)
		Cut	248 (239 … 258)	7.9 (6.4 … 9.9)
mc-Si	180 µm	*Wire*	90 (89 … 91)	21.5 (17.5 … 26.4)
		Cut	243 (234 … 253)	7.6 (6.1 … 9.5)
	160 µm	*Wire*	88 (86 … 90)	15.2 (12 … 19.3)
		Cut	257 (250 … 265)	11 (8.7 … 13.9)
	140 µm	*Wire*	84 (82 … 86)	15.2 (12.1 … 18.9)
		Cut	250 (241 … 259)	7.9 (6.4 … 9.8)

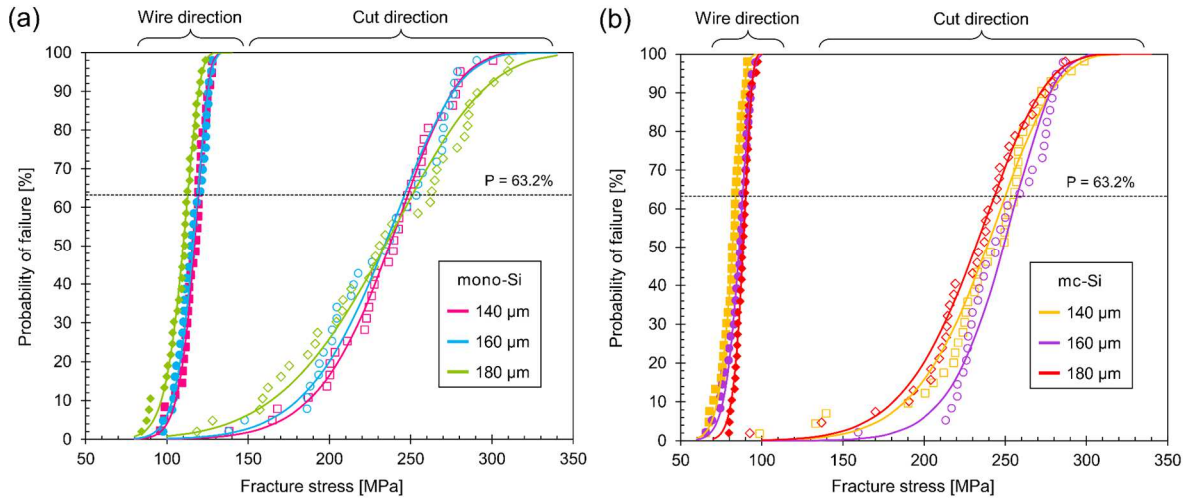

Fig. 11. Weibull probability failure plots for (a) monocrystalline and (b) multicrystalline wafers tested in *wire* and *cut direction*

The proposed interpretation to explain the difference in mechanical strength depending on loading direction is based on the orientation of the stress with respect to the characteristic defects of the wafers. Indeed, the mechanical resistance of as-cut wafers is mainly determined by the surface and edge defects induced by the sawing process. For diamond-sawn wafers in particular, these defects appear in the form of long grooves and indentation pits [17], which can be observed on the topographical maps on Fig. 10. As was previously introduced by Bidiville et al. [49], the grooves can be considered as through cracks, as they run over the total length of the wafer, and the pits are generally elongated in the direction of the wire. Now, in 4-line bending tests, as silicon is a brittle material sensitive to cracking, its failure is driven by tension rather than compression. This means that fracture will initiate on the side exposed to tensile stress, and more specifically, according to Weibull theory, where the largest defect is located. The direction of the tensile stress is always perpendicular to that of the support and loading rollers. Positioning the rollers parallel or perpendicular to the sawing marks therefore creates a fundamental difference in the way the defects are mechanically stressed. This difference in defect orientation with respect to the loading direction was previously reported by Yang et al [29] and more recently by Sekhar et al. [50] and is illustrated schematically in Fig. 12. When the wafer is bent in *wire direction*, the tensile stress acts perpendicular to the grooves and indentation pits while in *cut direction*, it is oriented parallel to the defects main orientation. It becomes then clear that in *cut direction*, the grooves are very unlikely to be the fracture origin. Indeed, as they already run over the total length of the wafer, they cannot propagate more in the direction in which they are being stressed (Fig. 12. b). This is however not the case when the sample is bent in *wire direction*: the grooves can easily be enlarged as they are stressed perpendicularly. Regarding the indentation pits, since the stress needed to propagate a crack is smaller when the load is applied perpendicular to the crack direction, their elongated shape explains that they are activated more rapidly when bent in *wire direction* than in *cut direction*. The combined effect of orientation of grooves and pits justifies the lower fracture strengths observed in *wire direction*.

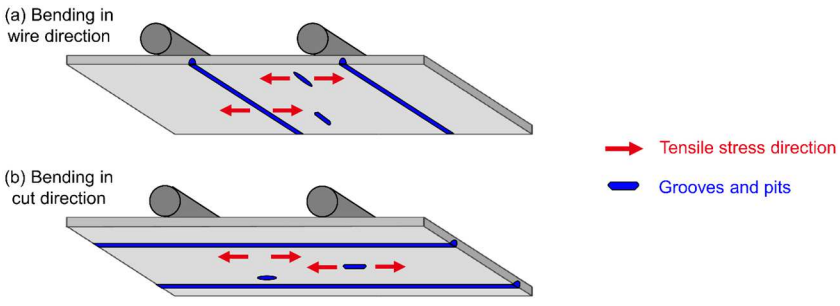

Fig. 12. Schematic representation of the orientation of tensile stress with respect to the characteristic defects at the wafer surface: (a) bending in *wire direction* (b) bending in *cut direction*

The orientation of the defects also allows us to propose an interpretation for the influence of the loading direction on the Weibull modulus (i.e. the scattering of the results). When bent in *wire direction*, the wafer can be seen as composed of many defects similar in geometry and density, which are all oriented in the direction most likely to initiate fracture. The critical stress values obtained show therefore very little scatter. However, when bent in *cut direction*, the number of the defects that are likely to cause fracture is smaller and may vary in shape and size. This therefore explains the large scattering of the stress values: if one wafer exhibits no indentation pit big enough or well oriented enough to be activated, it can hold up to 300 MPa, whereas another wafer can fail at 120 MPa if a large pit is present between the two rollers.

4.2.2. Influence of the wafer thickness

The major observation that can be made from Fig. 11 is that for a given loading direction and silicon type, the failure probability plots of different thicknesses almost perfectly overlap, i.e. both the Weibull modulus *m* and the characteristic fracture strength σ_θ do not vary with thickness. A constant Weibull modulus implies that the defect distribution is the same for all thicknesses, and hence that cutting thinner wafers does not modify the density of defects. Observing similar characteristic strength values means that the maximum stress value that a wafer can hold before failure is the same for thicknesses 180, 160 and 140 µm. It is however worth specifying that with decreasing wafer thickness, the breakage load decreases while the breakage displacement increases (Fig. 5), which explains why the maximum breakage stress remains constant. This result proves that increasing the ratio of the sawing-induced damage layer to the total wafer thickness does not alter the overall mechanical strength of the wafer. The characteristic fracture stress σ_θ and Weibull modulus *m* of a series of wafers are parameters that are thus representative of the material quality (bulk and surface) and the type of loading applied, but are independent of the thickness, at least down to 140 µm.

4.2.3. Influence of the silicon crystallinity

The comparison of the characteristic strength values shows that when bent in *cut direction*, mono-Si and mc-Si wafers exhibit a similar mechanical resistance (Fig. 13. a). In contrast, mc-Si wafers are significantly weaker than mono-Si wafers in *wire direction*. The characteristic strength σ_θ calculated for mc-Si wafers is indeed in average 25% less than for mono-Si wafers. On the other hand, no statistically significant difference can be observed regarding the Weibull modulus *m*.

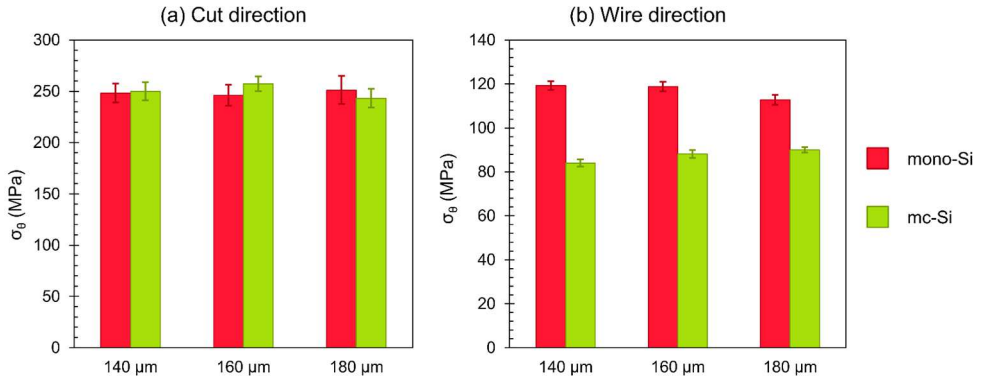

Fig. 13. Characteristic fracture strength and 90% confidence bounds of mono-Si and mc-Si wafers of different thicknesses tested in 4-line bending in (a) *cut* and (b) *wire direction*

The comparable strength values obtained for mono-Si and mc-Si wafers in *cut direction* indicate that when loading the wafers perpendicular to the sawing marks, the crystallinity does not play a role in the mechanical strength of the wafers. More specifically, bulk defects such as grains boundaries or twin boundaries that are present in multicrystalline wafers do

not lower their mechanical resistance. Therefore, the critical defects responsible for wafer fracture are not volume defects, but rather surface defects. Since both the mono-Si and mc-Si wafers were cut using the same processing parameters, their surface defects are similar and the strength value at which they are activated is the same. This is in agreement with the confocal microscope analysis presented in Section 4.1, which revealed that the surface morphologies were the same regardless of the wafer crystallinity, i.e. the average depth and density of the microscopic surface defects were similar for mono-Si and mc-Si wafers.

However, if only the surface defects were responsible for fracture, then there should be no difference either in mechanical resistance in *wire direction* between mono-Si and mc-Si wafers. The proposed explanation is that the lower strength of mc-Si wafers in *wire direction* comes from a difference in damage that is more likely to be found on subsurface regions of the wafers. Such investigations could not yet be carried out for this study, but this hypothesis is supported by a few previous studies. Buchwald et al. studied beveled samples from DWS mono-Si and mc-Si wafers and showed that the subsurface cracks were 15% deeper for mc-Si wafers [51]. More recently, Kumar et al. compared the subsurface damage induced by diamond wire scribing on the surface of mono-Si and mc-Si [22]. They found that when using the same abrasive, the scribed surface morphologies of mono-Si and mc-Si were similar, but the subsurface damage was different: no subsurface cracks were observed in mono-Si, whereas several complex median and lateral cracks formed in mc-Si. These subsurface cracks could be the origin of fracture when mc-Si wafers are loaded in *wire direction*, thus explaining their lower mechanical strength.

It is nevertheless certain that the mechanical resistance of mc-Si wafers in *wire direction* is not satisfactory. In particular, the maximum deflection values reached by the 140 µm samples before failure, in the order of 3 mm, may be too critical for industrial-scale handling operations.

4.3. Fracture pattern investigation

In order to gain a better understanding of the fracture mode of wafers in 4-line bending, several wafers were prepared according to the procedure described in Section 3.5 prior to testing. Because the differences in maximum deflection between *wire* and *cut direction* are all the more pronounced for thin wafers, we have chosen to prepare six mono-Si wafers and six mc-Si of thickness 140 µm. Half of the wafers were tested until fracture in *wire direction* and the other half in *cut direction*. The obtained samples were then observed with integrated photoluminescence imaging.

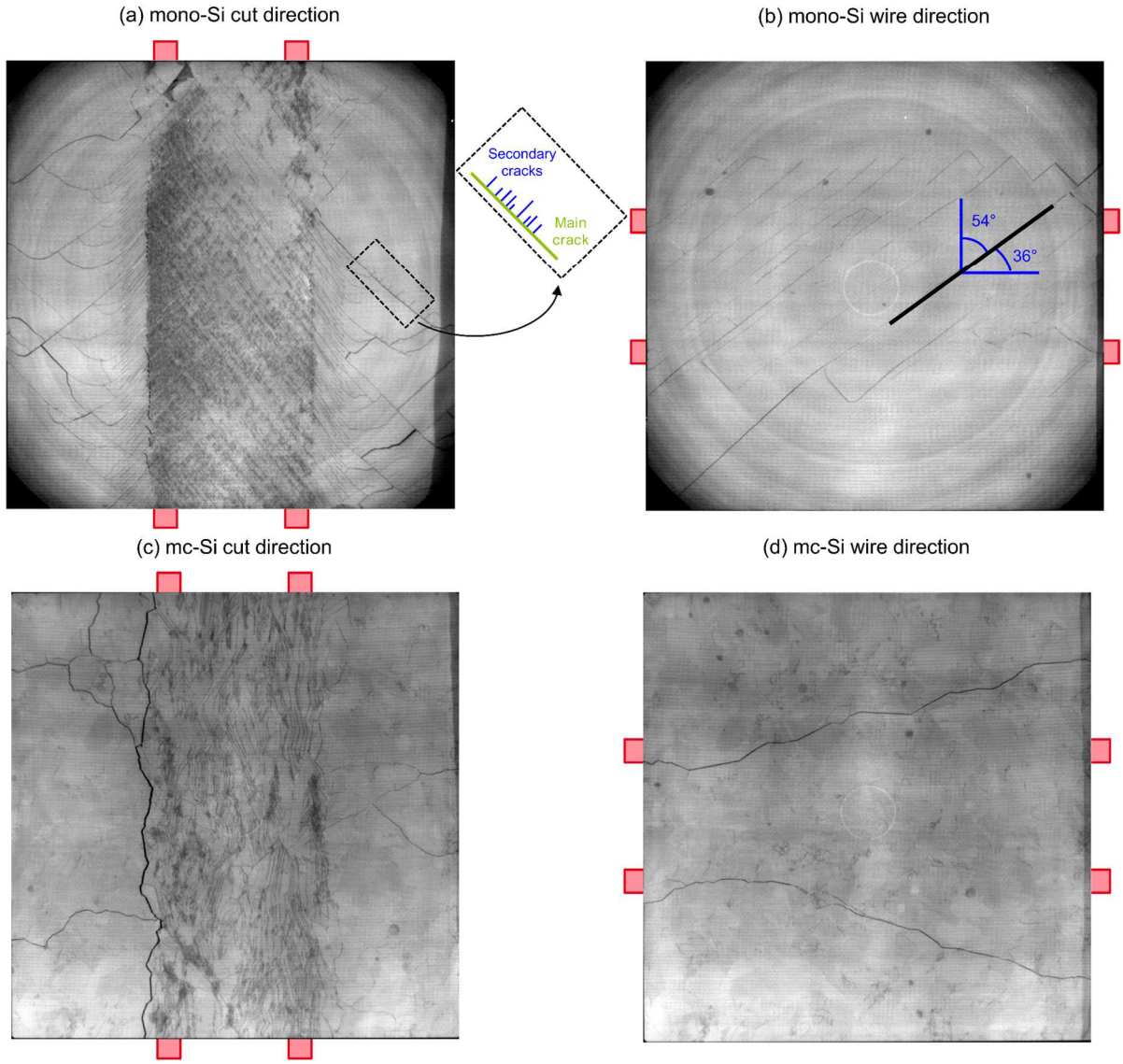

Fig. 14. Photoluminescence images of mono-Si and mc-Si 140 µm wafers broken in 4-line bending in *wire* and *cut direction* - the position of the loading rollers is schematically represented

The typical fracture patterns obtained for each silicon type and loading direction are shown in Fig. 14. For a better interpretation of the results, the position of the loading rollers (48 mm span) is schematically represented. It is worth specifying that this experimental technique does not provide information as to where the fracture started. It helps visualize the number of cracks and their main orientations, but it cannot determine which crack appeared first.

The first observation that can be made when looking at all patterns is that the cracks are always located in between the loading rollers, thereby confirming that the fracture initiates in the area where the stress is maximal. In mono-Si wafers, it sometimes appears that secondary cracks initiate from the main cracks, as illustrated on Fig. 14.c.

The particularity of mono-Si wafers is that their cracks are always oriented in a preferred direction, with an angle of approximately 54° (or 36°) with respect to the sides of the wafer, as illustrated on Fig. 14.b. These angle values are unexpected, as silicon is reported to have two privileged cleavage planes: the {110} and {111} planes [52], both of which are oriented at 45° with respect to the sides of the wafers. So a crack propagating in {110} or {111} planes should also be oriented at 45° to the sides of the wafers. The measurements performed on all images of broken mono-Si wafers confirm that for the test configuration considered in this study, crack propagation does not take place in {110} - or {111} - planes, and that the crack

direction is instead systematically oriented at about 10° with respect to the <110> direction, as illustrated in Fig. 15.

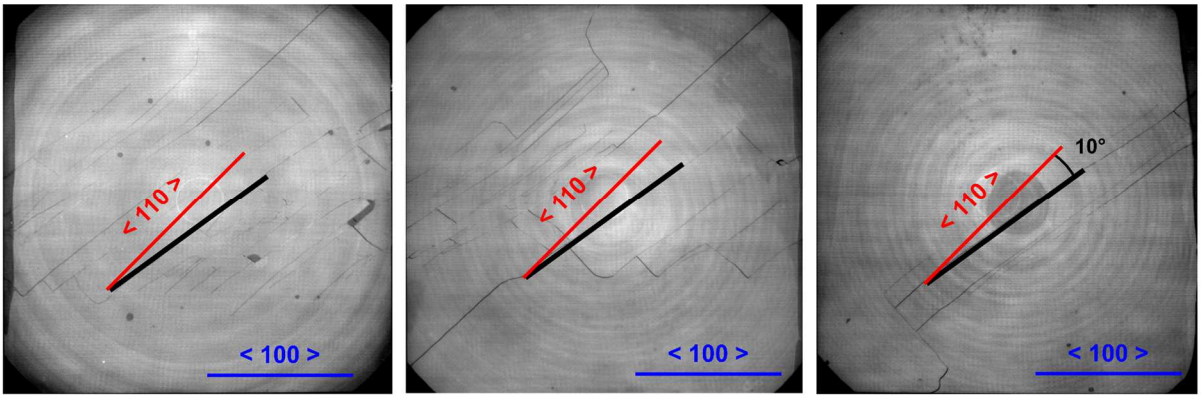

Fig. 15. Additional photoluminescence images of mono-Si wafers broken in 4-line bending in *wire direction* - the black line represents the cracks preferred orientation, while the red and blue line indicate the <110> and <111> directions

The reason for this specific crack orientation can be understood when considering the direction of the applied tensile stress with respect to the cleavage planes of the silicon wafer. Indeed, most of the works studying crack propagation in mono-Si via bending tests [53–55] use samples with sides oriented along the <110> direction, which can easily be obtained without laser cutting by natural cleavage of the plates. When testing such samples in 4-line bending, the {110} cleavage planes are oriented perpendicular to the tensile stress direction (Fig. 16.a). The crack (or more often the introduced pre-crack) can therefore easily propagate in the <110> direction, as it is loaded in mode I (opening mode, see Fig. 17) along the wafer length.

However, the wafers used in this study have their sides oriented along the <100> directions and the {110} cleavage planes thus form an angle of 45° with the stress direction (Fig. 16.b). Therefore, while the crack should normally preferably propagate at 45°, the orientation of the tensile stress creates a mixed-mode fracture (I + II + III) and the crack is deviated from the {110} planes.

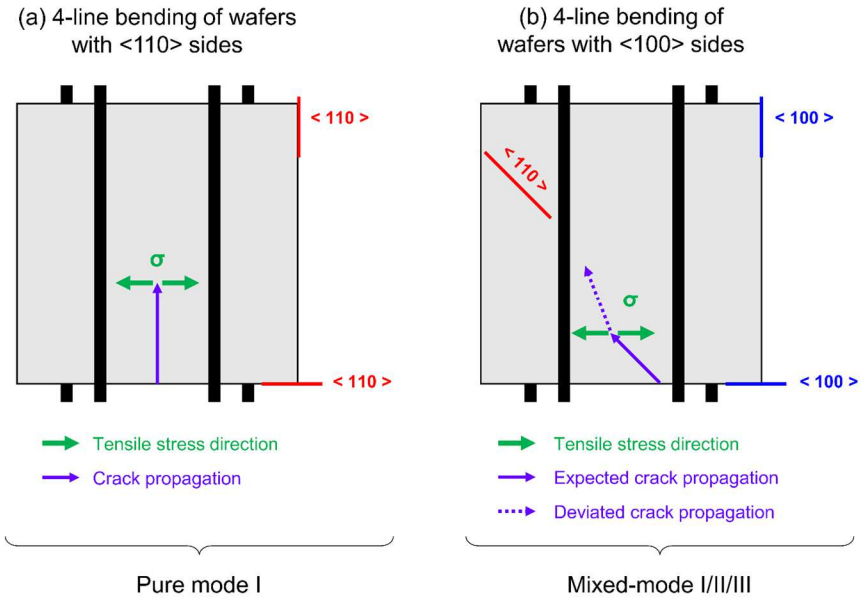

Fig. 16. Crack propagation mode in 4-line bending test with respect to the privileged cleavage directions for (a) a wafer with <110> sides and (b) a wafer with <100> sides

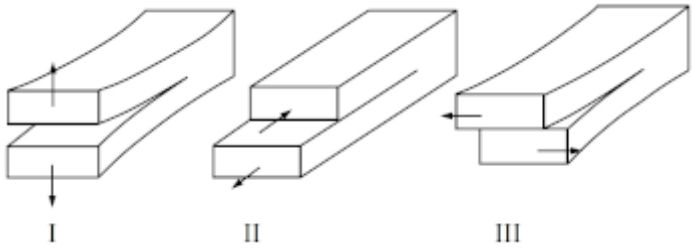

Fig. 17. The three elementary fracture modes

In contrast, the cracks in mc-Si follow more random orientations, and they regularly change direction as they propagate. This can be explained by the fact that the fracture path in mc-Si is mainly transgranular, i.e. the cracks propagate straightly in each grain and then change direction when crossing a grain boundary [56].

Despite their difference in crack orientation, the fracture mechanism in *cut direction* appears to be relatively similar for mono-Si and mc-Si wafers. They both exhibit an extremely dense and branching network of cracks between the loading rollers, which seem to indicate that the wafer stored a lot of energy as it deformed, and suddenly broke into hundreds of pieces with multiple cracks initiating almost simultaneously. In *wire direction*, the differences between mono-Si and mc-Si wafers are more distinct. Mc-Si wafers break into very few pieces (between three and six), and it is very easy to rebuild the path followed by the main cracks. In the case of mono-Si wafers, at least a dozen fragments can be identified in the fracture pattern. Moreover, the crack path is more complicated to recover: although several cracks seem to propagate parallel to each other, they occasionally follow a zigzag trajectory and cross each other.

5. Conclusions

The goal of this study was to investigate the mechanical properties of as-cut diamond-sawn silicon wafers, with a focus on the evolution of the mechanical resistance with decreasing wafer thickness. We presented an original slicing and sampling method to obtain comparable silicon wafers of two different silicon types (mono-Si and mc-Si) and three different thicknesses (140, 160 and 180 µm). The mechanical strength of the wafers was evaluated by means of 4-line bending tests coupled with FE simulations. The samples were characterized

before fracture by means of confocal microscopy, and the fracture patterns of some samples were analyzed after failure. The main findings of this study are reported as follows:

(1) All wafers tested exhibit a strong anisotropy in mechanical properties. The mechanical strength of wafers loaded perpendicular to the saw marks is twice as high than in parallel loading for mono-Si wafers, and three times as high for mc-Si wafers. This anisotropy can be explained by the orientation of the stress applied with respect to the sawing-induced defects at the surface of the wafers.
(2) For a given silicon type and loading direction, we found that wafers of different thicknesses showed the same breakage stress distribution. At least until 140 µm, the maximum stress that a wafer can withstand before failure depends on the crystal quality, the slicing process and the type of loading applied, but is independent of its thickness.
(3) Although mono-Si and mc-Si showed similar mechanical strength when loaded perpendicular to the saw marks, mc-Si wafers are significantly weaker than mono-Si wafers in parallel bending. We showed that the microscopic surface defects were not the cause of this difference, as the observed morphologies and roughness parameters of mono-Si and mc-Si wafers were similar. As supported by recent studies, the reason for the lower strength of mc-Si wafers in *wire direction* is more likely to be found in a difference in subsurface damage rather than in surface defects.
(4) Study of the fracture patterns shows that the cracks in mono-Si wafers do not propagate along the expected {110} cleavage planes. They are instead systematically oriented in a direction with an offset of approximately 10° with respect to the <110> direction. We show that this deviation is caused by the orientation of the tensile stress with respect to the {110} cleavage plane, which creates a mixed-mode fracture of the crack.

These results tend to confirm that the slicing process, and thus the quality of the surface and subsurface obtained, is the key step that defines the mechanical strength of a silicon wafer. Investigations on the influence of different slicing parameters, such as wire speed, abrasive size, cutting speed, will be essential in order to manufacture thinner wafers that are still mechanically reliable. In addition, these parameters need to be adjusted to the crystallinity of the silicon brick, as it was highlighted that monocrystalline and multicrystalline wafers that were cut using the same conditions can exhibit similar surfaces but significant differences in mechanical behavior. Future work should complement the obtained results with dynamic loading tests, as these are more representative of the loadings applied to a wafer during the handling operations that occur in the PV manufacturing chain.

Acknowledgments

This work was supported by the French Environment and Energy Management Agency (ADEME), which is gratefully acknowledged.

References

[1] L. Bekalé, S. Barazzouk, N. Sakai, T. Murakami, K. Miyoshi, T. Miyasaka, S. Hotchandani, Solution-processed tBu $_4$ -ZnPc:C $_{61}$ bulk heterojunction organic photovoltaic cells, Jpn. J. Appl. Phys. 55 (2016) 032301. doi:10.7567/JJAP.55.032301.
[2] J.S. Shaikh, N.S. Shaikh, A.D. Sheikh, S.S. Mali, A.J. Kale, P. Kanjanaboos, C.K. Hong, J.H. Kim, P.S. Patil, Perovskite solar cells: In pursuit of efficiency and stability, Mater. Des. 136 (2017) 54–80. doi:10.1016/j.matdes.2017.09.037.
[3] International Technology Roadmap for Photovoltaic (ITRPV), 10th edition, 2019.
[4] A. Kumar, S. Melkote, Diamond wire sawing of solar silicon wafers: a sustainable manufacturing alternative to loose abrasive slurry sawing, in: 15th Glob. Conf. Sustain. Manuf., Elsevier, 2018: pp. 549–566. doi:10.1016/j.promfg.2018.02.156.
[5] F. Coustier, J.-D. Penot, G. Sanchez, M. Ly, Diamond wire sawing - State of the art and perspectives (2012).pdf, Photovolt. Int. 15 (2012) 40–45.

[6] H. Wu, S.N. Melkote, Effect of crystal defects on mechanical properties relevant to cutting of multicrystalline solar silicon, Mater. Sci. Semicond. Process. 16 (2013) 1416–1421. doi:10.1016/j.mssp.2013.05.016.
[7] B. Meinel, T. Koschwitz, J. Acker, Textural development of SiC and diamond wire sawed sc-silicon wafer, Energy Procedia. 27 (2012) 330–336. doi:10.1016/j.egypro.2012.07.072.
[8] O. Anspach, B. Hurka, K. Sunder, Structured wire: From single wire experiments to multi-crystalline silicon wafer mass production, Sol. Energy Mater. Sol. Cells. 131 (2014) 58–63. doi:10.1016/j.solmat.2014.06.008.
[9] R. Koepge, K. Buehler, F. Kaule, J. Zeh, S. Schoenfelder, O. Anspach, Analysis of structured wire wafering processes to predict optimized process settings by varying particle size and wire diameter, AIP Conf. Proc. 1999 (2018) 140001. doi:10.1063/1.5049340.
[10] F. Kaule, B. Köhler, J. Hirsch, S. Schoenfelder, D. Lausch, Improved mechanical strength and reflectance of diamond wire sawn multi-crystalline silicon wafers by inductively coupled plasma (ICP) etching, Sol. Energy Mater. Sol. Cells. 185 (2018) 511–516. doi:10.1016/j.solmat.2018.05.057.
[11] A. Kumagai, Texturization using metal catalyst wet chemical etching for multicrystalline diamond wire sawn wafer, Sol. Energy Mater. Sol. Cells. 133 (2015) 216–222. doi:10.1016/j.solmat.2014.11.008.
[12] A. Kumar, S.N. Melkote, Wear of diamond in scribing of multi-crystalline silicon, J. Appl. Phys. 124 (2018) 065101. doi:10.1063/1.5037106.
[13] International Technology Roadmap for Photovoltaic (ITRPV), 9th edition, 2018.
[14] A. Bidiville, K. Wasmer, R. Kraft, C. Ballif, Diamond wire-sawn silicon wafers-from the lab to the cell production, in: Proc. 24th EU PV-SEC, 2009: pp. 1400–1405.
[15] T. Suzuki, Y. Nishino, J. Yan, Mechanisms of material removal and subsurface damage in fixed-abrasive diamond wire slicing of single-crystalline silicon, Precis. Eng. 50 (2017) 32–43. doi:10.1016/j.precisioneng.2017.04.011.
[16] C. Yang, H. Wu, S. Melkote, S. Danyluk, Comparative Analysis of Fracture Strength of Slurry and Diamond Wire Sawn Multicrystalline Silicon Solar Wafers, Adv. Eng. Mater. 15 (2013) 358–365. doi:10.1002/adem.201200262.
[17] E. Cai, B. Tang, W.R. Fahrner, L. Zhou, Characterization of the surfaces generated by diamond cutting of crystalline silicon, in: Proc. 26th Eur. Photovolt. Sol. Energy Conf. Exhib. EU PVSEC, 2011: pp. 1884–1886.
[18] A. Kumar, S. Kaminski, S.N. Melkote, C. Arcona, Effect of wear of diamond wire on surface morphology, roughness and subsurface damage of silicon wafers, Wear. 364–365 (2016) 163–168. doi:10.1016/j.wear.2016.07.009.
[19] A. Kumar, A. Kovalchenko, V. Pogue, E. Pashchenko, S.N. Melkote, Ductile Mode Behavior of Silicon During Scribing by Spherical Abrasive Particles, Procedia CIRP. 45 (2016) 147–150. doi:10.1016/j.procir.2016.02.341.
[20] A.M. Kovalchenko, Studies of the ductile mode of cutting brittle materials (A review), J. Superhard Mater. 35 (2013) 259–276. doi:10.3103/S1063457613050018.
[21] H. Wu, S.N. Melkote, Effect of crystallographic orientation on ductile scribing of crystalline silicon: Role of phase transformation and slip, Mater. Sci. Eng. A. 549 (2012) 200–205. doi:10.1016/j.msea.2012.04.034.
[22] A. Kumar, S.N. Melkote, S. Kaminski, C. Arcona, Effect of grit shape and crystal structure on damage in diamond wire scribing of silicon, J. Am. Ceram. Soc. 100 (2017) 1350–1359. doi:10.1111/jace.14732.
[23] A.M. Kovalchenko, S. Goel, I.M. Zakiev, E.A. Pashchenko, R. Al-Sayegh, Suppressing scratch-induced brittle fracture in silicon by geometric design modification of the abrasive grits, J. Mater. Res. Technol. (2018). doi:10.1016/j.jmrt.2018.05.016.
[24] B. Sopori, P. Basnyat, S. Devayajanam, R. Schnepf, S. Sahoo, J. Gee, F. Severico, A. Manens, H. Seigneur, W.V. Schoenfeld, Analyses of diamond wire sawn wafers: Effect of various cutting parameters, in: 2015 IEEE 42nd Photovolt. Spec. Conf. PVSC, IEEE, 2015: pp. 1–6.

[25] S. Würzner, A. Falke, R. Buchwald, H.J. Möller, Determination of the impact of the wire velocity on the surface damage of diamond wire sawn silicon wafers, Energy Procedia. 77 (2015) 881–890. doi:10.1016/j.egypro.2015.07.124.
[26] T. Liu, P. Ge, W. Bi, Y. Gao, Subsurface crack damage in silicon wafers induced by resin bonded diamond wire sawing, Mater. Sci. Semicond. Process. 57 (2017) 147–156. doi:10.1016/j.mssp.2016.10.021.
[27] A. Kumar, S.N. Melkote, The chemo-mechanical effect of cutting fluid on material removal in diamond scribing of silicon, Appl. Phys. Lett. 111 (2017) 011901. doi:10.1063/1.4991536.
[28] H. Meng, L. Zhou, Mechanical Behavior of Diamond-Sawn Multi-Crystalline Silicon Wafers and its Improvement, Silicon. 6 (2014) 129–135. doi:10.1007/s12633-013-9170-2.
[29] C. Yang, F. Mess, K. Skenes, S. Melkote, S. Danyluk, On the residual stress and fracture strength of crystalline silicon wafers, Appl. Phys. Lett. 102 (2013) 021909. doi:10.1063/1.4776706.
[30] H. Sekhar, T. Fukuda, Y. Kida, K. Tanahashi, H. Takato, The impact of damage etching on fracture strength of diamond wire sawn monocrystalline silicon wafers for photovoltaics use, Jpn. J. Appl. Phys. 57 (2018) 126501. doi:10.7567/JJAP.57.126501.
[31] A. Kumar, R.G.R. Prasath, V. Pogue, K. Skenes, C. Yang, S.N. Melkote, S. Danyluk, Effect of Growth Rate and Wafering on Residual Stress of Diamond Wire Sawn Silicon Wafers, Procedia Manuf. 5 (2016) 1382–1393. doi:10.1016/j.promfg.2016.08.108.
[32] A. Kumar, K. Skenes, R.G.R. Prasath, C. Yang, S.N. Melkote, S. Danyluk, Spatial distribution of full-field residual stress and its correlation with fracture strength of thin silicon wafers, in: Proc. 28th Eur. Photovolt. Sol. Energy Conf. Exhib. EU PVSEC, 2013: pp. 1474–1476.
[33] V.A. Popovich, A. Yunus, M. Janssen, I.J. Bennett, I.M. Richardson, Effect of microstructure and processing parameters on mechanical strength of multicrystalline silicon solar cells, in: 35th IEEE Photovolt. Spec. Conf., 2010: pp. 2222–2226.
[34] A. Kumar, C. Yang, S. Melkote, S. Danyluk, Relationship between Macro- scale and Micro- scale Mechanical Properties of Photovoltaic Silicon wafers, in: Proc. 29th Eur. Photovolt. Sol. Energy Conf. Exhib. EU PVSEC, 2014: pp. 769–772.
[35] P. Wang, X. Yu, Z. Li, D. Yang, Improved fracture strength of multicrystalline silicon by germanium doping, J. Cryst. Growth. 318 (2011) 230–233. doi:10.1016/j.jcrysgro.2010.11.081.
[36] F. Kaule, W. Wang, S. Schoenfelder, Modeling and testing the mechanical strength of solar cells, Sol. Energy Mater. Sol. Cells. 120 (2014) 441–447. doi:10.1016/j.solmat.2013.06.048.
[37] C. Borri, M. Gagliardi, M. Paggi, Fatigue crack growth in Silicon solar cells and hysteretic behaviour of busbars, Sol. Energy Mater. Sol. Cells. 181 (2018) 21–29. doi:10.1016/j.solmat.2018.02.016.
[38] J.J. Hall, Electronic effects in the elastic constants of n-type silicon, Phys. Rev. 161 (1967) 756.
[39] C. Funke, E. Kullig, M. Kuna, H.J. Möller, Biaxial Fracture Test of Silicon Wafers, Adv. Eng. Mater. 6 (2004) 594–598. doi:10.1002/adem.200400406.
[40] L. Zhao, A. Maynadier, D. Nelias, Stiffness and fracture analysis of photovoltaic grade silicon plates, Int. J. Solids Struct. 97–98 (2016) 355–369. doi:10.1016/j.ijsolstr.2016.07.013.
[41] S. Saffar, S. Gouttebroze, Z.L. Zhang, Fracture Analysis and Distribution of Surface Cracks in Multicrystalline Silicon Wafers, J. Sol. Energy Eng. 136 (2014) 021024.
[42] S. Schoenfelder, A. Bohne, J. Bagdahn, Comparison of test methods for strength characterization of thin solar wafer, in: Proc. 22nd Eur. Photovolt. Sol. Energy Conf., 2007: pp. 1636–1640.
[43] V.A. Popovich, W. Geerstma, M. Janssen, I.J. Bennett, I.M. Richardson, Mechanical Strength of Silicon Solar Wafers Characterized by Ring-On-Ring Test in Combination with Digital Image Correlation, in: EPD Congr. 2015, Springer, 2015: pp. 241–248.

[44] N. Watanabe, T. Miyazaki, K. Yoshikawa, M. Aoyagi, Damage Evaluation of Wet-Chemical Si-Wafer Thinning/Backside Via Exposure Process, IEEE Trans. Compon. Packag. Manuf. Technol. 4 (2014) 741–747. doi:10.1109/TCPMT.2014.2304462.
[45] ASTM International, Standard Test Method for Flexural Strength of Advanced Ceramics at Ambient Temperature, ASTM C 1161, (2018).
[46] A.S. Azar, B. Holme, Ø. Nielsen, Effect of sawing induced micro-crack orientations on fracture properties of silicon wafers, Eng. Fract. Mech. 154 (2016) 262–271. doi:10.1016/j.engfracmech.2016.01.014.
[47] DIN SPEC 91351: Strength testing for photovoltaic wafers, (2017).
[48] W. Weibull, A statistical distribution function of wide applicability, J. Appl. Phys. 18 (1951) 293–297.
[49] A. Bidiville, J. Heiber, K. Wasmer, S. Habegger, F. Assi, Diamond wire wafering: wafer morphology in comparison to slurry sawn wafers, in: Proc. 25th Eur. Photovolt. Sol. Energy Conf., 2010.
[50] H. Sekhar, T. Fukuda, K. Tanahashi, K. Shirasawa, H. Takato, K. Ohkubo, H. Ono, Y. Sampei, T. Kobayashi, The impact of saw mark direction on the fracture strength of thin (120 µm) monocrystalline silicon wafers for photovoltaic cells, Jpn. J. Appl. Phys. 57 (2018) 095501. doi:10.7567/JJAP.57.095501.
[51] R. Buchwald, K. Fröhlich, S. Würzner, T. Lehmann, K. Sunder, H.J. Möller, Analysis of the Sub-surface Damage of mc- and cz-Si Wafers Sawn with Diamond-plated Wire, Energy Procedia. 38 (2013) 901–909. doi:10.1016/j.egypro.2013.07.363.
[52] R. Pérez, P. Gumbsch, Directional anisotropy in the cleavage fracture of silicon, Phys. Rev. Lett. 84 (2000) 5347.
[53] D. Sherman, I. Be'ery, Velocity dependent crack deflection in single crystal silicon, Scr. Mater. 49 (2003) 551–555. doi:10.1016/S1359-6462(03)00354-3.
[54] L. Zhao, D. Bardel, A. Maynadier, D. Nelias, Crack initiation behavior in single crystalline silicon, Scr. Mater. 130 (2017) 83–86. doi:10.1016/j.scriptamat.2016.11.015.
[55] M. Wang, L. Zhao, M. Fourmeau, D. Nelias, Crack plane deflection and shear wave effects in the dynamic fracture of silicon single crystal, J. Mech. Phys. Solids. 122 (2019) 472–488. doi:10.1016/j.jmps.2018.09.031.
[56] L. Zhao, D. Nelias, D. Bardel, A. Maynadier, P. Chaudet, B. Marie, On the fracture of multi-crystalline silicon wafer, J. Phys. Appl. Phys. 49 (2016) 475601. doi:10.1088/0022-3727/49/47/475601.